V. Lauth, M.Maas, K. Rezwan

An evaluation of colloidal and crystalline properties of CaCO3 nanoparticles for biological applications

Journal Article as: peer-reviewed accepted version (Postprint)

DOI of this document*(secondary publication): 10.26092/elib/2484

Publication date of this document: 18/09/2023

* for better findability or for reliable citation

Recommended Citation (primary publication/Version of Record) incl. DOI:

V. Lauth, M. Maas, K. Rezwan,
An evaluation of colloidal and crystalline properties of CaCO3 nanoparticles for biological applications,
Materials Science and Engineering: C, Volume 78, 2017, Pages 305-314, ISSN 0928-4931,
https://doi.org/10.1016/j.msec.2017.04.037.

An evaluation of colloidal and crystalline properties of $CaCO_3$ nanoparticles for biological applications

V. Lauth [a], M. Maas [a,b,*], K. Rezwan [a,b]

[a] Advanced Ceramics, University of Bremen, Am Biologischen Garten 2, 28359 Bremen, Germany
[b] MAPEX — Centre for Materials and Processes, University of Bremen, Bremen 28359, Germany

ARTICLE INFO

Article history:
Received 7 February 2017
Received in revised form 5 April 2017
Accepted 6 April 2017
Available online 7 April 2017

Keywords:
Crystallinity
Solubility
Colloidal stability
Phase-transformation
Cytotoxicity
Cellular uptake
Drug delivery

ABSTRACT

Biodegradable calcium carbonate carriers are a promising and safe nanoparticle platform which might enable various applications as an engineered nanomaterial in health care, food and cosmetics. However, engineered nanoparticles can exhibit new forms of toxicity that must be carefully evaluated before being widely adopted in consumer products or novel drug delivery systems. To this end, we studied four common calcium carbonate particle systems (calcite nanoparticles, amorphous sub-micrometer and vaterite sub-micrometer and micrometer particles) and compared their behavior in biological medium and in cell culture experiments. The thermodynamically stable calcite phase is shown to maintain its morphological features as no phase transformation occurs. Size- and time-dependent phase transformation of the less stable vaterite particles are observed within 96 h in cell medium. The protein serum albumin can be an effective inhibitor of phase-transition and it is shown to improve colloidal stability. The impact of the biological environment goes beyond protein-corona formation, as we observed rapid dissolution of amorphous particles in high ionic strength cell medium, but not in Millipore water. Cellular responses of human osteoblasts against $CaCO_3$ particles indicate that increased intracellular calcium ions improve viability and that particle internalization is not size-dependent. Useful insights for designing $CaCO_3$-based delivery systems are provided and also corroborate to the idea that intrinsic material properties as well as environmental conditions are of relevance for the successful implementation of dispersed $CaCO_3$ particles in drug delivery systems and in other applications.

1. Introduction

The use of engineered nanoparticles (ENPs) in consumer products is becoming increasingly prevalent [1]. Clothing [2], cosmetic [1] and food industries [3] are just a few examples of today's use of ENPs. The particles are mainly applied as pigments and fillers, for the occlusion and delivery of active ingredients and as antimicrobial agents. Another field in which the use of nanoparticles holds great potential is nanomedicine [4,5], especially considering tumor targeting, diagnostics, imaging and treatment [6]. With the increasing use of ENPs, the necessity for nanosafety assessments is well recognized [2], as evidenced by the strong increase in the publications numbers within the past two decades [7].

As a consequence of various strategies to trick the immune system, like change of particle aspect ratio or functionalization with stealth polymers and self-peptides, these colloidal systems are able to avoid clearance [8,6,9]. Accordingly, these materials can exhibit new forms of toxicity, especially as a result of long-term accumulation in the body [10]. To avoid such undesirable effects, biodegradable and biocompatible materials are a promising option. Food and Drug Administration (FDA)-approved polymers like chitosan and poly(lactate) (PLGA) received special attention as they are well tolerated by the body [9]. Another alternative is the use of endogenous materials, like calcium phosphate, calcium carbonate and phosphosilicates [11]. Calcium carbonate ($CaCO_3$) holds great potential, as it is highly pH-sensitive and dissociates into calcium and carbonate ions, which already are ubiquitous in the body.

$CaCO_3$ exists in six different crystal morphologies: the naturally occurring calcite, aragonite, vaterite and amorphous calcium carbonate (ACC) phase and the highly unstable ikaite and monohydrocalcite. Only calcite is thermodynamically stable, while aragonite and vaterite are slightly unstable and tend to transform into calcite in the presence of water/humidity [12–14]. The same is true for amorphous calcium carbonate which in nature often occurs as a precursor to the more stable polymorphs [15]. All $CaCO_3$ polymorphs have a certain solubility in water which is determined by the solubility product and scales with the thermodynamic stability of each crystal phase [16]. This instability is more pronounced at the nanoscale, at which solubility and reactivity increases due to an enhanced surface to volume ratio [17]. Additionally, the dissolution rate is known to be highly dependent on the intrinsic

* Corresponding author at: MAPEX — Centre for Materials and Processes, University of Bremen, Bremen 28359, Germany.
E-mail address: michael.maas@uni-bremen.de (M. Maas).

http://dx.doi.org/10.1016/j.msec.2017.04.037

nature of the particles (composition and crystal phase) [15] as well as on the environmental conditions (pH, presence of proteins and calcium-chelating moieties, ionic strength) [18–20]. Moreover, the dissolution of nanoparticles in biological medium can impact the biological systems interacting with the material, potentially changing the toxicity behavior from nano to ion-related [7]. Given that, to properly design $CaCO_3$-based drug delivery systems (DDS) or similar nanostructures with dispersed $CaCO_3$ particles considering particle solubility in the respective media is critical. Furthermore, colloidal stability and consequently biological availability of $CaCO_3$ particles could be influenced by their crystal phase and morphology as a consequence of different surface properties of the nanomaterials including their interactions with media biomolecules.

As a result of the detailed and inspired studies of $CaCO_3$ biomineralization, a vast number of publications report the design of $CaCO_3$ particles for drug delivery. However, just for a fraction of these publications in vitro or in vivo studies were performed [21–65]. The latter studies evaluated different aspects of the $CaCO_3$-cellular interactions: intracellular behavior [36,65], pH modulation [37], bubble generation [34,35,53], bone remodeling [24], photothermal therapy [22,28,43,49], drug/protein delivery [21,23,25–27,29–33,38,41,42,46–48,50–52,60–62], gene transfection [44,45,54–59], cellular uptake [63], toxicity [40,65] and bioavailability studies [39,64,65]. Among these publications, crystalline particles like calcite, vaterite and aragonite [38] phases have been utilized. These particle-systems varied in size from bulk material, to micrometer (1–1.5 μm), sub-micrometer (150–800 nm) and nanometer (30–100 nm) particles. In the case of amorphous carriers, the range of particle size was narrower, from 100 to 230 nm [44–49]. In some cases, the interplay of both amorphous and crystalline $CaCO_3$ phases was also reported [24,41–43]. In others, the crystallinity of the particles was not described [50–65]. Moreover, the aforementioned systems were tested with different cell culture media, incubation periods and cell lines. While most studies report viable nanoparticle systems in their own context, comparing the results is a challenging task. The lack of standardization when assessing biological responses [66] along with the incomplete information on the colloidal characterization makes it difficult to generalize the results, especially considering the real-live performance of particle-based drug delivery systems.

With the above discussion in mind, we designed a study that would allow us to compare the biological behavior of different $CaCO_3$ systems with varied crystallinity, solubility and colloidal properties. To this end, we analyzed the material properties of four different types of $CaCO_3$ particles commonly described in the literature as potential drug delivery systems and investigated their biological behavior against human osteoblasts in the Dulbecco's Modified Eagle's Medium (DMEM). Here, we focused on the changes in material properties in the cell medium and on the impact of the particles on the cells. For our study, we chose calcite, ACC particles and vaterite particles in the range of 90 nm to 1 μm which we consider representative in regards to polymorphism and size of those described in the literature as potential drug delivery systems.

2. Materials

Calcium chloride ($CaCl_2$ dihydrate, purity > 96%), sodium carbonate (Na_2CO_3, purity > 99.5%), poly(acrylic acid) sodium salt (PAA, M_w 8000 g/mol, 45 wt% in water), bovine serum albumin (BSA, lyophilized powder), glycerol (Gly, purity > 99.5%), sodium hydrogencarbonate ($NaHCO_3$, purity > 99.5%), ethylene glycol (EG, purity ≥ 99%) were purchased from Sigma-Aldrich and used without further purification. The experiments were performed using double deionized water with a conductivity of 0.04 mS cm^{-1} from Synergy (Millipore, Darmstadt, Germany).

Cell culture tests were carried out on human osteoblast cells (HOB, lot no. 232R020412 obtained from Provitro - Germany). Dulbecco's Vogt modified Eagle's minimal essential medium (DMEM, high glucose), antibiotic-antimycotic (AB/AM), Alexa Fluor 488 phalloidin (AF488) were obtained from Invitrogen (Germany). Fetal calf serum (FCS), phosphate buffered saline (PBS), trypsin-ethylenediaminetetraacetic acid (0.25% trypsin, 0.02% EDTA), Triton X-100, 4′,6-diamidino-2-phenylindole (DAPI, 0.5 μg/mL), paraformaldehyde (PFA, 95.0–100.5%), osmium tetroxide solution (OsO_4, 4% in water), glutaraldehyde solution (Grade 1, 25% in water) and an epoxy embedding medium kit (Epon 812 substitute) were purchased from Sigma-Aldrich (Germany). The water-soluble tetrazolium salt (WST-1) cell toxicity assay (Roche Diagnostics GmbH, Germany) and the lactate dehydrogenase (LDH) Pierce assay (Thermo Scientific, Germany) were directly purchased from the suppliers.

2.1. Synthesis of crystalline and amorphous nanoparticles

Calcite nanoparticles, purchased from PlasmaChem GmbH (Berlin, Germany) are produced by a sol-gel process and used as purchased. Amorphous particles were prepared as previously described [67]. In short, 10 mL aqueous solution with a final concentration of 1.9 g/L of PAA and 12 mM of $CaCl_2$ was prepared. To mineralize the particles, an aqueous solution of Na_2CO_3 was added to the reach the final concentration of 12 mM. The suspension was centrifuged at 5000 rpm for 10 min, the supernatant discarded and particles dried in an oven at 70 °C for 1 h.

Vaterite particles were prepared in a similar way as previously reported [37,68–70]. Micrometer particles were synthesized in a water:EG solution (1:6, v/v). First, 207 μL of 2 M $CaCl_2$ aqueous solution was first added to 4.15 mL of EG solution, stirred for 5 min and followed by 415 μL of 1 M $NaHCO_3$ aqueous solution and 227 μL of water. The final concentration of carbonate was kept equimolar at 83 mM. The solution turned turbid after 5 min, indicating the formation of particles. After 1 h stirring at 500 rpm, 30 mL of 100% ethanol was added to the suspension. Particles were collected by centrifugation at 5000 rpm for 10 min. This washing step was repeated twice and the collected particles were dried at 70 °C for 2 h. Sub-micrometer particles were prepared in a similar fashion but with a few modifications. The 1:6 water:EG solution was substituted by water:EG:Gly 1:1.25:3.7 in volume. Both $CaCl_2$ and $NaHCO_3$ aqueous solutions were added to a 4.15 mL solution containing 1.04 mL of EG and 3.11 mL of Gly. The final concentration of calcium and carbonate was kept equimolar at 83 mM. The solution remained transparent for about 1 h. The dispersion turned turbid after this period. Particles were collected by centrifugation after 2 h 30min, followed by washing the particles twice in 100% ethanol and drying at 70 °C for 2 h. For experiments without BSA-stabilization, the particles were dispersed in the respective medium in an ultrasound bath for 10 min.

2.2. Particle-stabilization by BSA

Dried particles were dispersed in 0.2% BSA in Millipore water to prepare 1.2 g/L particle concentration. The suspension was ultrasonicated for 15 min to ensure that no aggregates remained in solution and to fully coat the particles. Afterwards, it was centrifuged for 10 min at 5000 rpm and dried at 70 °C for 1 h.

2.3. Calcium-ion release from nanoparticles

The calcium content in the supernatant was quantified using the o-cres-olphthalein complexone colorimetric kit (Fluitest CA-CPC). Briefly, an amount of dried particles were added to the respective medium to prepare a particle concentration of 1.2 g/L. The suspension was serially diluted in the same medium to prepare 0.6, 0.3, 0.15 and 0.075 g/L. The suspensions were centrifuged for 10 min at 5000 rpm. 10 μL of the supernatant was added to a 96-well plate containing 50 μL of reaction mixture 1 (reagent obtained in the kit). 50 μL of reaction mixture 2 was added and the well plate was shaken for 30 s to allow homogeneous mixing. The plate was incubated for 10 min at room temperature (RT) and the absorbance was measured at 570 nm with plate reader.

The calcium concentration was calculated using a standard curve by a serial dilution of the 2.5 mM standard acquired with the kit.

2.4. Toxicity profile assessment

To assess toxicity of the $CaCO_3$ particles, cell viability at different concentrations was tested in a similar way to [71], by means of membrane integrity via LDH release (Pierce assay) and metabolic activity via mitochondrial activity (WST-1 assay, Roche). Particles stabilized by BSA were centrifuged and sterilized overnight under a UV lamp and redispersed in DMEM at different concentrations. Human osteoblast cells (4th to 11th passage) were cultured in DMEM supplemented with 10% heat-inactivated FCS and 1% antibiotics/antimicotics in an incubator (C200, Labotect Labor Technik, Germany) at 37 °C with 10% CO_2 and 95% relative humidity (RH). One day prior to the experiments, the cells were detached and seeded in a 24-well plate at a density of 2×10^4 cells per well. On the following day, the dispersions were added and incubated for 24 h. In addition, for the WST-1 assay, cells grown in culture medium were set as high control (100% cell viability), and others incubated with Triton X-100 (2%, w/v) were used as low control (0% cell viability). For the LDH assay, the cytotoxicity was calculated relative to Triton X-100 as high control and cells in culture medium as low control. Samples were measured in triplicates and evaluated as mean and standard deviations (SD).

2.4.1. Particle uptake studied via electron microscopy

For Transmission electron microscopy (TEM) analysis, a similar procedure to [72] was used. Shortly, osteoblasts were washed once with PBS, detached with trypsin/EDTA and transferred to 2 mL Eppendorf cups. The cups were centrifuged at 6000 rpm for 6 min, fixed with standard 2.5% glutaraldehyde, 2.5% formaldehyde in 0.1 M Na-cacodylate for 1 h at RT. After removal of the fixative, the cells were washed several times with phosphate buffer and post-fixed with Osmium tetroxide solution for 1 h at RT. The black pellet was washed twice and dispersed in 2% agar (Sigma-Aldrich) in Millipore water, and allowed to solidify at 4 °C. The pellet in agar was cut into squares of about 1 mm wide. The blocks were dehydrated in a graded series with ethanol (twice for 5 min in 30% and 50% ethanol, 3 times for 10 min in 70%, 90% and twice for 15 min in 100% ethanol). Blocks were embedded in Epon 812. Ultrathin sections were taken with an ultramicrotome (Ultracut R, Leica, Wetzlar, Germany). No surface markers were used (uranyl acetate or ruthenium red), in order to enhance the contrast of intracellular components, as these are not the focus of the analysis.

2.5. Characterization techniques

For the measurement of particle size and zeta-potential, dried particles were ultrasonicated for 10 min in the respective medium. Particle size and zeta potential were determined by a Zetasizer after 4 h of incubation (Malvern Instruments, Nano ZSP). The data is given as mean ± standard deviation (SD) based on three independent measurements. The aggregation behavior was evaluated in terms of the particle size distribution and polydispersity index (PDI). The morphology of the carriers was evaluated by scanning electron microscopy (Zeiss, SUPRA 40), with an acceleration voltage of 15 kV as well as transmission electron microscopy with a Zeiss EM 900 (Zeiss, Oberkochen, Germany) at 80 kV. Images were acquired using a CCD-camera (TRS, Dünzelbach, Germany) with the software ImageSP (TRS). X-ray diffraction (XRD) analysis was carried out using a JSO-Debyeflex 2002 device, with Cu K α radiation ($\lambda = 1.542$ Å). The samples were ground to a powder, placed on the holder with silicone grease and scanned from 20° to 50°, 1 s per step. UV-Vis spectroscopy was performed on a Multiskan Go device (Thermo Scientific). Thermogravimetric measurements (TGA) were performed in STA 503 (Bähr Thermoanalyse) with a heating rate of 4 °C/min under 2 L/min of atmospheric air. The specific surface area (SBET) of the samples was determined by nitrogen adsorption (Belsorp-Mini, Bel Japan, Osaka, Japan), using the BET-method. The pore size distribution was determined by the BJH method from the adsorption/desorption hysteresis of the BET-isotherms.

3. Results

3.1. Material characterization of the $CaCO_3$ particles

The $CaCO_3$ particles were fully characterized prior to the cell experiments. Fig. 1 shows a TEM overview of the particles immediately after synthesis (vaterite and ACC) or as purchased (calcite). The calcite particles are monodisperse and exhibit a rhombohedral shape with a particle size of 90 ± 10 nm. The amorphous particles are synthesized in Millipore water by the complex coacervation of [Ca^{2+}] ions and PAA, followed by mineralization with Na_2CO_3, as previously reported by us [67]. As the size can be controlled by complexation time and PAA concentration, the smallest particle size that can be obtained with this method is 250 ± 20 nm in diameter. Due to the nature of the synthesis, smaller nanoparticles (8 nm particles in diameter) are also formed [73]. Vaterite particles are prepared in a water-solvent mixture [37,68–70]. Sub-micrometer particles are prepared in 1:1.25:3.7 water:EG:Gly in volume ratio and yield particles size of 600 nm ± 20 nm while micrometer particles are prepared in 1:6 water:EG, which yields 1 μm ± 0.1 μm particles. Supporting Fig. 1 shows an XRD analysis of the crystal phases of calcite and vaterite particles, as well as the absence of reflexes in the amorphous phase. BJH characterization of the samples showed that both vaterite particles are porous, with a mean pore diameter of 7 nm for sub-micrometer and 9 nm for micrometer, respectively (Supporting Fig. 2). The amorphous sub-micrometer particles as well as calcite nanoparticles are not porous.

3.2. Time-dependent phase-transformation in DMEM

It is well known that thermodynamically metastable phases tend to transform into more stable phases, like calcite [15]. This transformation is triggered in the presence of water/moisture [12] and can be a concern when designing $CaCO_3$-based DDSs. To analyze the phase-transformation in cell culture medium and to assess the influence of protein-

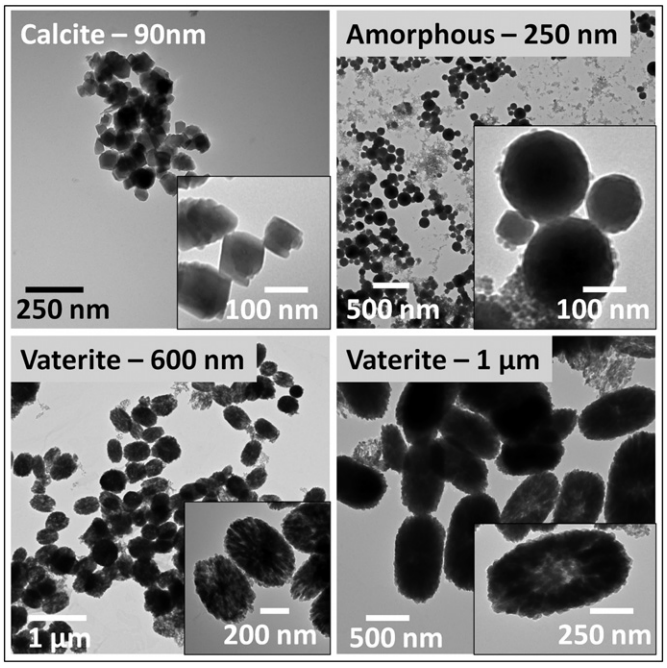

Fig. 1. TEM overview of calcite, amorphous, micrometer and sub-micrometer vaterite particles. Crystalline and amorphous particles are dispersed in Millipore water while vaterite particles in ethanol.

coating in this transformation, $CaCO_3$ particles were dispersed in DMEM and SEM images were taken at 24 and 96 h after initial dispersing.

The SEM analysis of the samples dispersed in DMEM for 24 and 96 h and with or without BSA-coating is summarized in Fig. 2. In the absence of BSA-stabilization, it was observed that calcite nanoparticles neither dissolve in DMEM nor grow within the time frame of the experiment. Moreover, the X-ray diffraction patterns (Supporting Fig. 3) confirm that calcite does not phase-transform within 96 h. For vaterite sub-micrometer particles, morphological changes at 96 h from rods to micrometer-sized, rhombohedral-shaped crystals indicate a phase transformation. This is also observed in the XRD data, where a peak at 29° indicates the complete transformation into the calcite phase. On the other hand, micrometer-sized vaterite particles do not phase-transform into calcite and maintain their morphology and size. Amorphous sub-micrometer particles are not shown in the picture because of their complete dissolution in DMEM.

The presence of BSA can act as a phase-stabilizer of less stable polymorphs. The shape and size of BSA-coated calcite nanoparticles and vaterite microparticles are not affected by the presence of the protein and both size and crystallinity remain constant throughout the experiment. As opposed to the BSA-free solution, BSA-stabilized sub-micrometer vaterite particles remain stable in solution for 96 h without appreciable change in shape or size. A closer inspection of the XRD data (Supporting Fig. 3) reveals that the rate of the transformation is drastically reduced by the protein coating. It is worth mentioning that the phase-transformation appears to be both size-dependent, as it just occurs in the sub-micrometer vaterite particles as well as time-dependent, as no phase transformation is observed after 24 h. This behavior can be explained by the higher surface-to-volume ratio of the smaller particles which goes along with higher instability and enhanced solubility [68]. For instance, the surface area of micrometer vaterite particles is 44 m^2/g, which is low compared to sub-micrometer sized particles with 104 m^2/g. Finally, the addition of BSA does not prevent the dissolution of the amorphous particles in DMEM.

3.3. Colloidal stability in different media

As shown above, the presence of proteins can alter the phase transformation of $CaCO_3$ particles in cell culture medium. The presence of BSA in medium and its adsorption at the surface of the nanoparticles directly affect the colloidal stability, as shown in Fig. 3. The physisorption of the protein can be quantified via thermogravimetry. In the absence of protein (Fig. 3a), calcite particles do not show a mass loss up to 600 °C. As the temperature rises, calcination takes place, which accounts for around 50% of the weight loss. Vaterite particles show a similar trend. Up to 200 °C, absorbed and intrinsic water are removed. Between 200 and 300 °C left-over solvents are removed, followed by a calcination reaction. The amorphous particles show the highest weight loss of about 70% ± 10%, from which around 20% can be attributed to absorbed water, 25% from PAA and 17% from calcination. By comparing the TGA data in the presence of proteins (Fig. 3d) it is possible to calculate the weight loss associated with protein absorption within the temperature range from 210 °C to 405 °C. For calcite nanoparticles, BSA accounts for 4.2 ± 3.1% of the weight loss. This relates to around 0.45 mM of BSA per g of particle. In the case of the micrometer vaterite particles, 3.1 ± 2.9% of the weight is related to BSA, which represents approximately 0.60 mM of BSA/g of particle. Sub-micrometer particles absorbed 5.0 ± 4.5% of its weight, around 0.75 mM of BSA/g of particle. Amorphous particles did not absorb any appreciable amount of protein.

$CaCO_3$ has an isolectric point around pH 6 in ultrapure water [74], and is therefore negatively charged at physiological pH. In Millipore water at pH 7 and in the absence of BSA, the dispersed calcite particles have a mean hydrodynamic diameter of 91 ± 16 nm (Fig. 3b) and show good colloidal stability (PDI 0.29) with a zeta-potential of −29.6 ± 2.3 mV (Fig. 3c). The amorphous particles also show good stability with the lowest zeta-potential in water, around −46.8 ± 3.6 mV, while the hydrodynamic size is 220 ± 35 nm. The high zeta-potential value can be explained by the inclusion of PAA molecules, which are negatively charged at neutral pH. The micron-sized vaterite particles

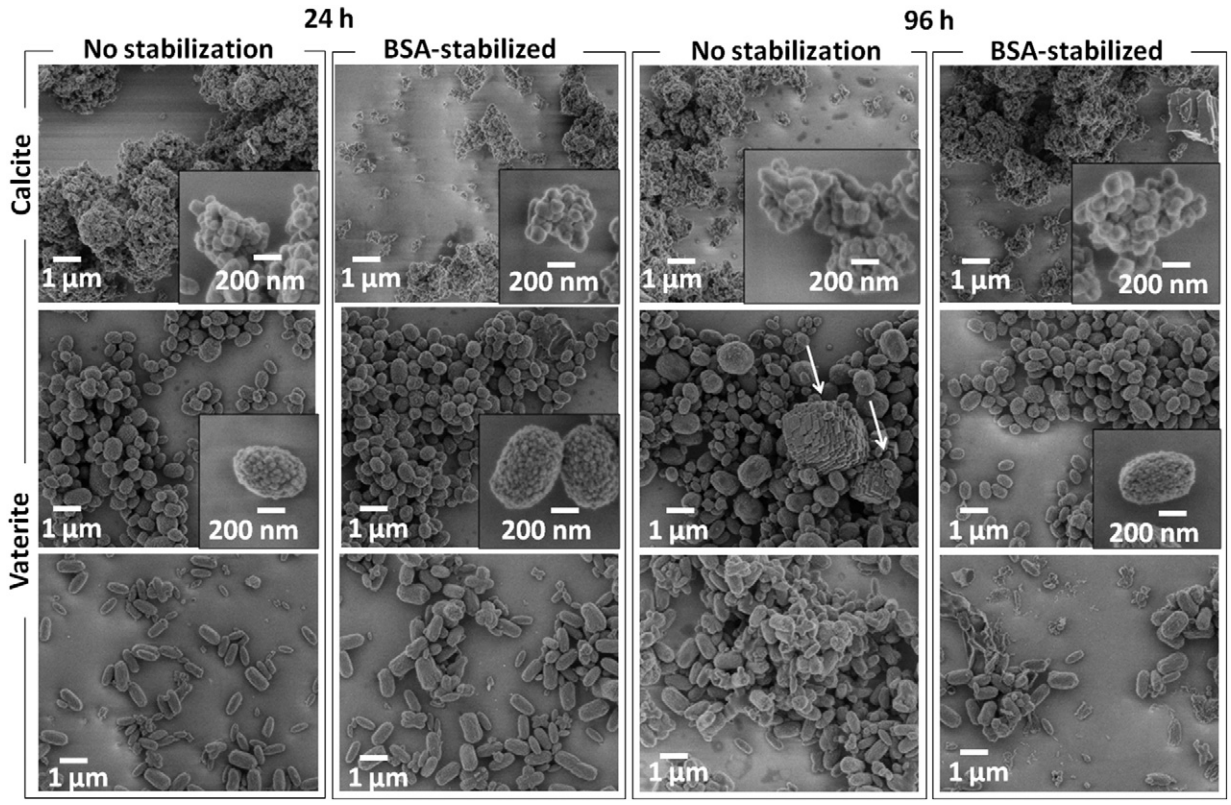

Fig. 2. SEM overview of calcite, amorphous, micrometer vaterite and sub-micrometer vaterite particles after 24 and 96 h of incubation in DMEM. Both bare and BSA-stabilized particles are reported. Amorphous particles immediately dissolved in DMEM and therefore are not shown. Arrows indicate the possible formation of calcite microcrystals.

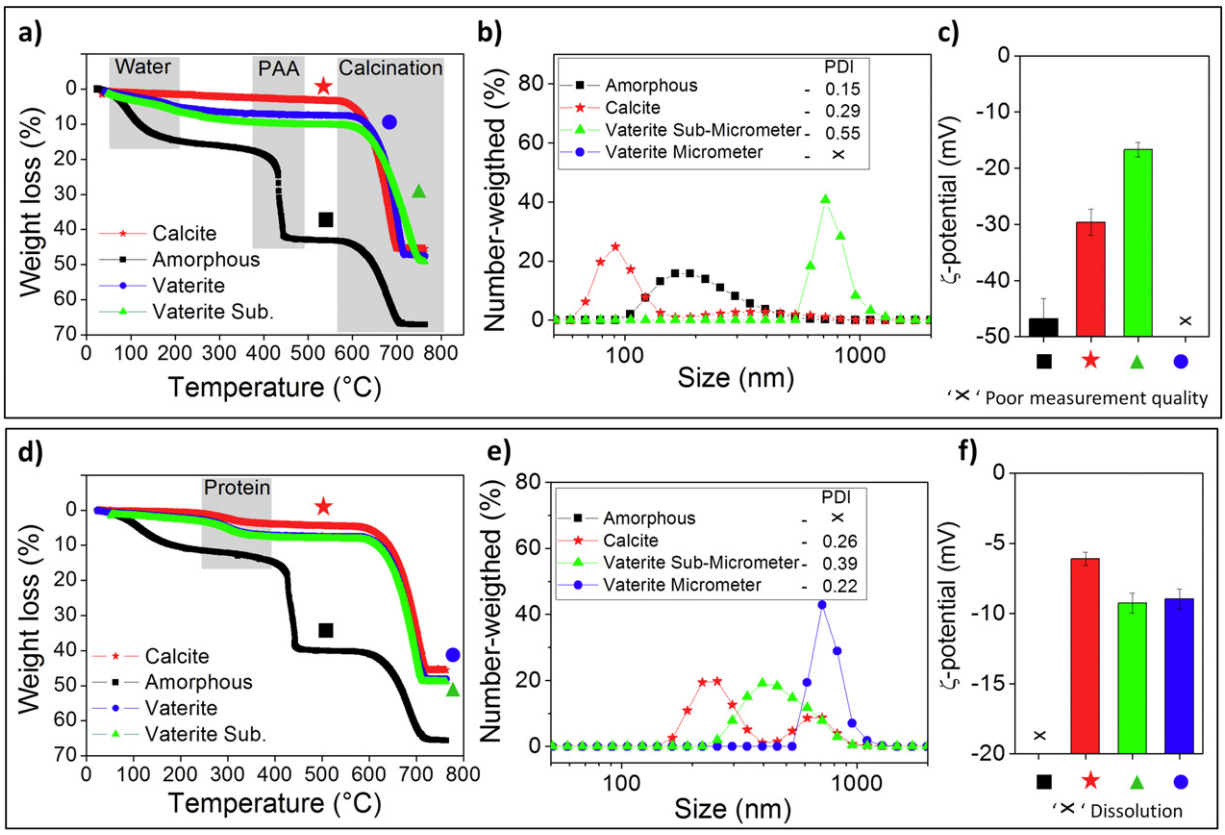

Fig. 3. Thermogravimetric analysis (a, d), number-weighted particle size distribution (b, e) and zeta-potential (c, f) of calcite, amorphous, micrometer and sub-micrometer vaterite particles. (a) Dried bare particles, (b–c) bare particles dispersed in Millipore water, (d) dried BSA-stabilized particles, and (e–f) BSA-stabilized particles dispersed in DMEM.

showed strong agglomeration and sedimentation in water which prevented accurate DLS measurements. The sub-micrometer vaterite particles have a hydrodynamic size of around 712 ± 40 nm and zeta-potential of −16.7 ± 1.3 mV.

When the bare particles (in absence of BSA) were dispersed in DMEM, rapid agglomeration and sedimentation took place and therefore DLS measurements were not possible. The instability can be related to the high ionic-strength of the medium, which reduces the Debye-length and the repulsion forces between nanoparticles [75]. On the other hand, BSA-stabilized suspensions are partially stable in DMEM, showing PDI values of around 0.3 and zeta-potential around −10 mV. In medium, the calcite dispersion exhibited a mean hydrodynamic diameter of 255 ± 30 nm (Fig. 3e) and a zeta-potential of −6.1 ± 1.0 mV (Fig. 3f). In contrast to dispersions in Millipore water, amorphous particles dissolved upon redispersion in DMEM. Note that this dissolution is not caused by a low pH, but is instead probably a result of chelating of Ca^{2+} ions by the various amino acids and phosphate salts contained in DMEM. Vaterite microparticles showed a size of 712 ± 50 nm and a zeta-potential of about −9.2 ± 1.0 mV. Sub-micrometer vaterite particles have a hydrodynamic size of around 396 ± 30 nm and a zeta-potential of −8.9 ± 1.0 mV. In DMEM, it is observed that the stabilization of particles with 3 to 5% of BSA can hinder aggregation and improve colloidal stability of all types of particles (Fig. 3b, c, e, f). These findings are also supported by a previous report [36].

3.4. Dissolution behavior in different media

As shown previously, the incorporation of BSA improves colloidal stability and slows down the rate of phase transformation of sub-micrometer vaterite particles. Serial dilution of particles along with determining the free calcium ions allowed us to examine the dissolution behavior of each particle type in both water and DMEM. In Millipore water, bare particles are tested while in DMEM, BSA-stabilized particles are used due to the improved colloidal stability. In water, all particles are stable with low calcium ion release (Fig. 4a). At 1.2 g/L, amorphous particles show the highest calcium ion release, approximately 1.2 ± 0.3 mM, followed by vaterite sub-micrometer particles at 0.9 ± 0.2 mM, calcite nanoparticles at 0.8 ± 0.2 mM and vaterite microparticles at 0.7 ± 0.1 mM.

If the particles are dispersed in DMEM, the minimum calcium concentration detected is 1.80 ± 0.2 mM, which corresponds to the calcium concentration in the medium (Fig. 4b). Crystalline particles remain stable and barely dissolve. The calcium concentration remains constant with values ranging around 1.8 mM for all different particle concentrations. Amorphous particles on the other hand, readily dissolve in DMEM, increasing the Ca^{2+} concentration up to 6.0 ± 0.3 mM at 1.2 g/L. The dissolution of amorphous particles is confirmed by turbidity measurements at 450 nm and by SEM. Moreover, additional experiments of BSA-coated particles in water and bare particles in DMEM (Supporting Fig. 4) revealed similar results.

3.5. Toxicity profile of $CaCO_3$ particles against HOBs

Toxicity experiments were performed using a HOB cell line and incubated with BSA-stabilized particles for 24 h in serum-free DMEM at different particle concentrations (Fig. 5). Two standard experiments were performed: the LDH release assay, which indicates membrane damage with increasing LDH release and hence toxicity, and the WST-1 assay which indicates viability by quantifying the mitochondrial activity of the investigated cells. Amorphous particles did not show any significant deviation from the control (pure medium) both for LDH release and for viability (Fig. 5a and b). However, it must be noted that for mitochondrial activity, the values approached 80% indicating a possible toxic effect of the amorphous particles or its constituents that are released upon

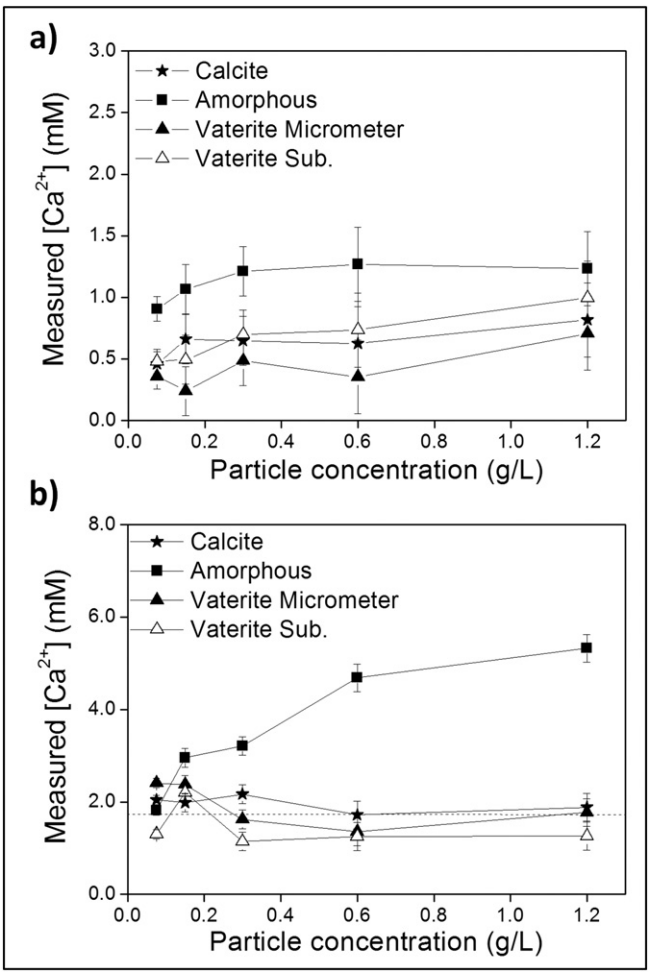

Fig. 4. Dissolution of calcite, micro- and sub-micrometer vaterite and amorphous particles upon serial dilution in aqueous medium. (a) Bare particles (no BSA-stabilization) dispersed in Millipore water pH 7. (b) BSA-stabilized particles dispersed in DMEM pH 7.4.

the already described dissolution of the particles in DMEM. Calcite particles displayed conflicting results. Regarding LDH release, a concentration-dependent increase in LDH release was observed. At higher particle concentration, 1.2 g/L, the LDH release showed significant values close to toxic levels (20%). On the contrary, viability experiments displayed improved viability, up to 125% at the highest particle concentration. Both types of vaterite particles show no significant deviations from the control for LDH release. Moreover, as with calcite, improvement in viability is observed for sub-micrometer particles at 0.6 g/L and at 1.2 g/L for micrometer-sized particles.

Control experiments were performed using $CaCl_2$ and PAA and are shown in Fig. 5c and d. Poly(acrylic acid) can be toxic depending on its molecular weight. According to the LDH release, no significant values are observed when compared to the control. However, the viability decreases considerably at 1.9 g/L of PAA, which is similar to the concentration of PAA used in the preparation of the amorphous particles. At lower concentrations, 0.15 and 0.7 g/L, no toxic effect can be observed. In the calcium chloride control experiments, optimal conditions for cell viability can be obtained by adding additional $CaCl_2$ up to 2 mM to DMEM medium, while higher concentrations reduce cell viability and also show an increase in membrane damage.

By comparing the experiments using Ca^{2+} as control and the ones with crystalline particles, better viability for crystalline particles is observed (around 150%) than for 0.5 mM [Ca^{2+}] as control (127 ± 15%). Since in both experiments the extracellular calcium is kept roughly the same, around 2 mM and 2.3 mM respectively, the difference in viability cannot just be explained by the elevation in the extracellular calcium concentration. Accordingly, due to the particle uptake followed by lysosomal dissolution (see below), the increase in intracellular calcium levels might cause even stronger cellular excitation, and therefore cellular viability.

Live-dead staining experiments were performed to validate the aforementioned experiments and the results are shown in Supporting Fig. 5. In these experiments with all particle types, all cell cultures are observed to be 100% viable for a particle concentration of 0.3 g/L. By analyzing fluorescent micrographs of cells incubated with 0.3 g/L of particles (Supporting Fig. 6), no morphological alterations were observed.

3.6. Particle-dependent uptake by human osteoblasts

Calcite nanoparticles are internalized by HOB cells, as observed on microtome sections analyzed via TEM (Fig. 6). As a result of trypsinization, the cells appeared to be spherical with a diameter of about 15 to 20 μm. Since the cells were not stained with surface markers for practical reasons, the identification of intracellular membranes was not optimized. Control experiments with cells incubated in the absence of particles also show spherical cells in which the mitochondria could be observed as a denser region (Supporting Fig. 7). The embedding resin that encloses the cell has a lighter colour, which allows for good distinction between cells and resin. When incubated with calcite nanoparticles, the size of the nanoparticles (90 nm) closely matches the size of the microtome slices (60–85 nm). Therefore, entire nanoparticles can remain in the slice and can be observed as dark dots in the TEM images. Internalized nanoparticles are located within endosomes. In the case of amorphous particles, which readily dissolved in DMEM, no particles can be observed within or outside the cells.

Due to the large size of the sub-micrometer and micrometer vaterite particles, these particles are shattered during slicing. What remains appears as an open space with a shape similar to the initial particles. As these spaces are transmitting, they appear as brighter regions dotted with remaining bits of $CaCO_3$ (dark dots). Both types of vaterite particles seem to be internalized and are located within endosomes.

Upon internalization, the particles can be dissolved in the acidic environment of the lysosomes. As discussed above, increased intracellular Ca^{2+} levels could be the reason for elevated mitochondrial activity as observed via the WST-1 assay (Fig. 5). Supporting Fig. 8 shows fluorescent micrographs of intracellular calcium stained with Fluo-3 AM. Analysis of the images indicates a higher calcium concentration in the cytosol than in the nucleus, but no clear significant distinction between the different particle types could be observed.

4. Discussion

The phase transformation of less stable phases to calcite is a phenomenon that occurs in air [12,14] and in aqueous solutions [13,68]. The observed phase transformation of sub-micrometer particles is a function of the increasing surface-to-volume ratio and overall free energy, with decreasing particle size. Moreover, the ion-exchange mechanism that leads to phase transformation is dependent on the diffusion rate, which is also enhanced with a higher surface-to-volume ratio [68]. The phase-transformation is usually accompanied by changes in morphology and size, which can alter the colloidal stability and the biological responses of crystalline particles. Our findings suggest that the adsorption of BSA on the surface of $CaCO_3$ crystals can hinder the phase transformation of sub-micrometer vaterite particles. These results are supported by previous studies [37], which stated that nanosized vaterite particles can be stabilized by 2% BSA in PBS. The use of proteins to modulate crystal precipitation, morphology and crystallinity is also observed in nature [76,77]. Accordingly, proteins and analogous polyionic polymers have been widely studied in the field of biomineralization for modifying crystal nucleation and growth [78]. Additionally, a series of proteins like BSA, R-chymotrypsin and lysozyme

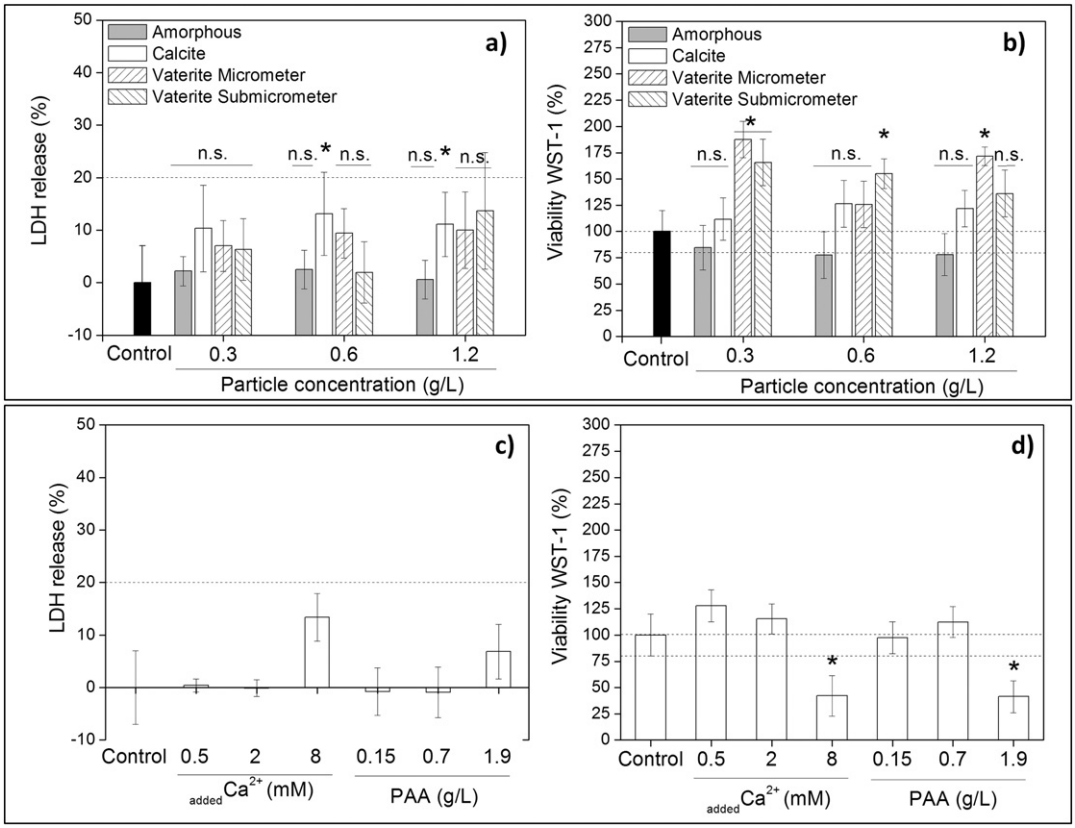

Fig. 5. HOB intracellular LDH release (a, c) and mitochondrial viability (b, d) when incubated with calcite, amorphous and vaterite particles at different particle concentration as well as with $CaCl_2$ and PAA. (a, b) incubation with BSA-stabilized particles. (c, d) control experiments using $CaCl_2$ and PAA. *Significant value $p < 0.05$, n.s. non significant value.

have been physically adsorbed to porous $CaCO_3$ microcrystals and studied as protein-delivery systems [79].

Colloidal stability in biological medium is also recognized as an important parameter for drug delivery systems [80]. It is also known that a reduction of the particle concentration in the nanometer range due to colloidal instability can result in lower cytoxicity profiles [81]. In Millipore water, nanometer and sub-micrometer $CaCO_3$ particles are well dispersed. However, micrometer vaterite particles did not yield stable suspensions as these large particles rapidly sediment. In DMEM, however, agglomeration and sedimentation is observed for all bare particle systems, due to the elevated ionic-strength of this medium and possibly due to adsorption of small molecules like sugars and amino acids present in DMEM. The increased ionic strength reduces both the Debye-Hückel length and the electro-static potential, hence the

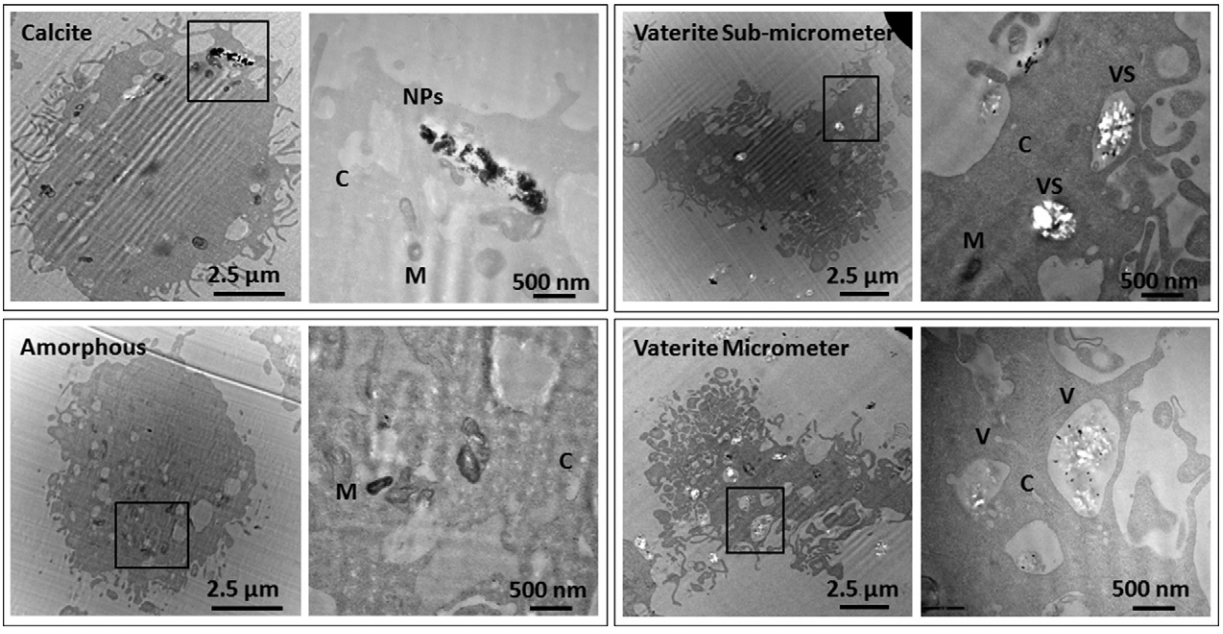

Fig. 6. TEM of HOB cells incubated with calcite, amorphous, sub-micrometer and micrometer vaterite particles for 24 h. Particle concentration: 0.3 g/L. Right panel is a high magnification image from selected area on left panel. Labels: C - cytosol, M - mitochondria, NPs - calcite nanoparticles, VS - vaterite sub-micrometer particles, V - vaterite microparticles.

repulsive force between nanoparticles, which can lead to destabilization [75]. It must be pointed out that the presence of divalent ions in DMEM (1.8 mM of calcium ions) can also significantly contribute to the destabilization in the cell medium [75]. On the other hand, BSA-stabilized suspensions are more stable in DMEM according to PDI values. This can partially be explained by the steric stabilization provided by the bulky BSA molecules. Similar stabilization provided by proteins was previously reported [36,82]. Finally, regarding the relationship between crystalline phases and the colloidal stability, no apparent role can be observed. Since the zeta potential of all types of BSA-stabilized $CaCO_3$ particles was very similar, colloidal stability seems to be mostly dependent on particle size and ionic strength.

The dissolution behavior of each particle-system was determined in both Millipore water pH 7 and DMEM pH 7.4. As dissolution is dictated by the solubility product of each $CaCO_3$ phase, it can be expected that less thermodynamically stable phases are more soluble than other phases [16,19]. Accordingly, amorphous particles in water partially dissolved and a low increase in the calcium ion concentration was detected. Crystalline phases barely dissolved, and the difference in the dissolution behaviors of calcite and vaterite was not strongly pronounced at our experimental conditions. It is well-known that additional molecules in the medium, such as calcium chelators (particularly leucine, lysine and phosphate salts in DMEM, but also reported for citrates and EDTA in other buffers [19]) can significantly alter the phase equilibrium, which we experimentally observed for amorphous particles in DMEM. Amorphous particles readily dissolved in DMEM increasing the $[Ca^{2+}]$ in the medium. However, beneath the crystalline phases, the differences seem to be insignificant.

Toxicity experiments revealed that increased $[Ca^{2+}]$ concentration of around 2 to 6 mM can improve cell viability, which is a similar concentration range as was reported elsewhere [83]. This behavior occurred for all three types of crystalline particles, but not for the amorphous particles, indicating that the observed increase in cell viability might be a result of cell internalization followed by lysosomal dissolution of the more stable $CaCO_3$ particles. For the amorphous particles, the release of the additive PAA, which was used to stabilize the amorphous phase, possibly caused membrane damage. Our findings are supported by [84], which described that PAA molecules (25 k mol/g) can actively disrupt cellular membrane of mammalian cells and cause cytotoxicity.

The TEM micrographs of HOB cells suggest that calcite and vaterite particles are internalized by the cells. In the micrometer range, the shape of $CaCO_3$ particles on the uptake by cervical carcinoma cells was studied [63]. It was suggested that the number of internalized particles is dependent on the aspect ratio of the particles. In regards to $CaCO_3$ in the nanometer scale, the uptake of nanoparticles by A549 cells was also observed [36]. However the role of crystallinity in the uptake has not yet been differentiated. Considering that all three particle-systems investigated here, apart from amorphous particles, were internalized, no clear dependency could be observed, regardless of size or crystallinity.

5. Conclusion

In summary, we examined four common types of dispersed calcium carbonate particles that are regularly studied as novel drug delivery systems and which might eventually find their way into health-related consumer products. Both crystallinity and environmental conditions (ionic strength, presence of proteins and chelators) play key roles in the colloidal behavior and phase-stability of $CaCO_3$ particles. However, since $CaCO_3$ is basically nontoxic and biocompatible, these aspects do not strongly affect their cellular response and toxicology profile. The behavior of the particles regarding their crystallinity, solubility and colloidal stability was evaluated by various standard methods for the characterization of nanomaterials and showed that the crystalline particles remained dispersed in solution, with no appreciable dissolution; however, the amorphous particles readily dissolved in the cell nutrition medium DMEM. It is worth mentioning that the sub-micrometer vaterite particles phase-transition into the more stable calcite phase accompanied by changes in particle size and shape. This change was only observed after 24 h and only for the smaller sub-micrometer vaterite particles. The addition of BSA generally improved colloidal stability in cell culture medium and diminished the rate of phase-transformation of the smaller vaterite particles. While the crystalline particles remained in solution with low release of calcium ions, the amorphous nanoparticles readily dissolved upon dispersion in DMEM, increasing the extracellular Ca^{2+} concentration. Two cellular responses were observed: increased mitochondrial activity induced by an internal increase of calcium ion concentration for crystalline particles, and cell death by membrane damage due to the presence of PAA in amorphous particles. Cellular uptake was observed for all crystalline particles, even the large micrometer-sized vaterite particles. Consequently, crystallinity, solubility and colloidal stability are key parameters for engineering $CaCO_3$ nanomaterials for biological applications and should also be factored into all assessments of the feasibility of new drug delivery systems.

Acknowledgement

We thank James Ziemah for assistance in the preparatory work and the DFG Research Training Group GRK 1860, 'Micro-, meso- and macroporous nonmetallic materials: fundamentals and applications' (MIMENIMA) for funding.

Appendix A. Supplementary data

Supplementary data to this article can be found online at http://dx.doi.org/10.1016/j.msec.2017.04.037.

References

[1] R. Kessler, Engineered nanoparticles in consumer products, Environ. Health Perspect. 119 (2011) 246–253.
[2] R. Foldbjerg, X. Jiang, T. Miclăuş, C. Chen, H. Autrup, C. Beer, Silver nanoparticles – wolves in sheep's clothing? Toxicol. Res. 4 (2015) 563–575.
[3] B.S. Sekhon, Food nanotechnology - an overview, Nanotechnol. Sci. Appl. 3 (2010) 1–15.
[4] D. Peer, J.M. Karp, S. Hong, O.C. Farokhzad, R. Margalit, R. Langer, Nanocarriers as an emerging platform for cancer therapy, Nat. Nanotechnol. 2 (2007) 751–760.
[5] E. Blanco, H. Shen, M. Ferrari, Principles of nanoparticle design for overcoming biological barriers to drug delivery, Nat. Biotechnol. 33 (2015) 941–951.
[6] E. Lepeltier, L. Nuhn, C.-M. Lehr, R. Zentel, Not just for tumor targeting: unmet medical needs and opportunities for nanomedice, Nanomedicine (London) 10 (2015) 3147–3166.
[7] H.F. Krug, Nanosafety research-are we on the right track? Angew. Chem. Int. Ed. 53 (2014) 12304–12319.
[8] K.P. García, K. Zarschler, L. Barbaro, J.A. Barreto, W. O'Malley, L. Spiccia, H. Stephan, B. Graham, Zwitterionic-coated "stealth" nanoparticles for biomedical applications: recent advances in countering biomolecular corona formation and uptake by the mononuclear phagocyte system, Small 10 (2014) 2516–2529.
[9] F. Lebre, C.H. Hearnden, E.C. Lavelle, Modulation of immune responses by particulate materials, Adv. Mater. (2016) 5525–5541.
[10] H.F. Krug, P. Wick, Nanotoxikologie - eine interdisziplinäre Herausforderung, Angew. Chem. 123 (2011) 1294–1314.
[11] T. Shen, Y. Zhang, A.M. Kirillov, B. Hu, C. Shan, W. Liu, Y. Tang, Versatile rare-earth oxide nanocomposites: enhanced chemo/photothermal/photodynamic anticancer therapy and multimodal imaging, J. Mater. Chem. B 4 (2016) 7832–7844.
[12] F. Konrad, F. Gallien, D.E. Gerard, M. Dietzel, Transformation of amorphous calcium carbonate in air, Cryst. Growth Des. 16 (2016) 6310–6317.
[13] Z. Zou, L. Bertinetti, Y. Politi, A.C.S. Jensen, S. Weiner, L. Addadi, P. Fratzl, W.J.E.M. Habraken, Opposite particle size effect on amorphous calcium carbonate crystallization in water and during heating in air, Chem. Mater. 27 (2015) 4237–4246.
[14] R.K. Pai, S. Pillai, J. Ihli, W.C. Wong, E.H. Noel, Y.-Y. Kim, A.N. Kulak, H.K. Christenson, M.J. Duer, F.C. Meldrum, Dehydration and crystallization of amorphous calcium carbonate in solution and in air, CrystEngComm 5 (2014) 3169.
[15] V. Radha, T.Z. Forbes, C.E. Killian, P.U.P. Gilbert, A. Navrotsky, Transformation and crystallization energetics of synthetic and biogenic amorphous calcium carbonate, Proc. Natl. Acad. Sci. U. S. A. 107 (2010) 16438–16443.
[16] L.N. Plummer, E. Busenberg, The solubilities of calcite, aragonite and vaterite in CO_2-H_2O solutions between 0 and 90 °C, and an evaluation of the aqueous model for the system $CaCO_3$-CO_2-H_2O, Geochim. Cosmochim. Acta 46 (1982) 1011–1040.

[17] M. Auffan, J. Rose, J.-Y. Bottero, G.V. Lowry, J.-P. Jolivet, M.R. Wiesner, Towards a definition of inorganic nanoparticles from an environmental, health and safety perspective, Nat. Nanotechnol. 4 (2009) 634–641.
[18] M.P. Monopoli, C. Åberg, A. Salvati, K.A. Dawson, Biomolecular coronas provide the biological identity of nanosized materials, Nat. Nanotechnol. 7 (2012) 779–786.
[19] K. Sawada, The mechanisms of crystallization and transformation of calcium carbonates, Pure Appl. Chem. 69 (1997) 921–928.
[20] F. Meder, S.S. Thomas, L.W. Fitzpatrick, A. Alahmari, S. Wang, J.G. Beirne, G. Vaz, G. Redmond, K.A. Dawson, Labeling the structural integrity of nanoparticles for advanced in situ tracking in bionanotechnology, ACS Nano 10 (2016) 4660–4671.
[21] A. Wang, Y. Yang, X. Zhang, X. Liu, W. Cui, J. Li, Gelatin-assisted synthesis of vaterite nanoparticles with higher surface area and porosity as anticancer drug containers in vitro, Chem. Aust. 81 (2016) 194–201.
[22] Q. Dong, J. Li, L. Cui, H. Jian, A. Wang, S. Bai, Using porous $CaCO_3$/hyaluronic acid nanocages to accommodate hydrophobic photosensitizer in aqueous media for photodynamic therapy, Colloids Surf. A Physicochem. Eng. Asp. 516 (2017) 190–198.
[23] T.N. Borodina, D.B. Trushina, I.V. Marchenko, T.V. Bukreeva, Calcium carbonate-based mucoadhesive microcontainers for intranasal delivery of drugs bypassing the blood-brain barrier, Bionanoscience 6 (2016) 261–268.
[24] E. Tolba, W.E.G. Müller, B.M. Abd El-Hady, M. Neufurth, F. Wurm, S. Wang, H.C. Schröder, X. Wang, High biocompatibility and improved osteogenic potential of amorphous calcium carbonate/vaterite, J. Mater. Chem. B 4 (2016) 376–386.
[25] J. Zhang, Y. Li, H. Xie, B.-L. Su, B. Yao, Y. Yin, S. Li, F. Chen, Z. Fu, Calcium carbonate nanoplate assemblies with directed high-energy facets: additive-free synthesis, high drug Loading, and sustainable releasing, ACS Appl. Mater. Interfaces 7 (2015) 15686–15691.
[26] N. Qiu, H. Yin, B. Ji, N. Klauke, A. Glidle, Y. Zhang, H. Song, L. Cai, L. Ma, G. Wang, L. Chen, W. Wang, Calcium carbonate microspheres as carriers for the anticancer drug camptothecin, Mater. Sci. Eng. C 32 (2012) 2634–2640.
[27] Y. Guo, W. Jia, H. Li, W. Shi, J. Zhang, J. Feng, L. Yang, Facile green synthesis of calcium carbonate/folate porous hollow spheres for the targeted pH-responsive release of anticancer drugs, J. Mater. Chem. B 4 (2016) 5650–5653.
[28] A. Neira-Carrillo, E. Yslas, Y.A. Marini, P. Vásquez-Quitral, M. Sánchez, A. Riveros, D. Yáñez, P. Cavallo, M.J. Kogan, D. Acevedo, Hybrid biomaterials based on calcium carbonate and polyaniline nanoparticles for application in photothermal therapy, Colloids Surf. B Biointerfaces 145 (2016) 634–642.
[29] Y. Zhao, Y. Lu, Y. Hu, J.-P. Li, L. Dong, L.-N. Lin, S.-H. Yu, Synthesis of superparamagnetic $CaCO_3$ mesocrystals for multistage delivery in cancer therapy, Small 6 (2010) 2436–2442.
[30] Y. Guo, J. Zhang, L. Jiang, X. Shi, L. Yang, Q. Fang, H. Fang, K. Wang, K. Jiang, Facile one-pot preparation of calcite mesoporous carrier for sustained and targeted drug release for cancer cells, Chem. Commun. (Camb.) 48 (2012) 10636–10638.
[31] V. Lauth, B. Loretz, C.M. Lehr, M. Maas, K. Rezwan, Self-assembly and shape control of hybrid nanocarriers based on calcium carbonate and carbon nanodots, Chem. Mater. 28 (2016) 3796–3803.
[32] G. Begum, T.N. Reddy, K.P. Kumar, K. Dhevendar, S. Singh, M. Amarnath, S. Misra, V.K. Rangari, R.K. Rana, An in situ strategy to encapsulate antibiotics in a Bio-inspired $CaCO_3$ structure enabling pH-sensitive drug release Apt for therapeutic and imaging applications, ACS Appl. Mater. Interfaces (2016).
[33] W. Wei, G.-H. Ma, G. Hu, D. Yu, T. McLeish, Z.-G. Su, Z.-Y. Shen, Preparation of hierarchical hollow $CaCO_3$ particles and the application as anticancer drug carrier, J. Am. Chem. Soc. 130 (2008) 15808–15810.
[34] D.J. Park, K.H. Min, H.J. Lee, K. Kim, I.C. Kwon, S.Y. Jeong, S.C. Lee, Photosensitizer-loaded bubble-generating mineralized nanoparticles for ultrasound imaging and photodynamic therapy, J. Mater. Chem. B 4 (2016) 1219–1227.
[35] K.H. Min, H.S. Min, H.J. Lee, D.J. Park, J.Y. Yhee, K. Kim, I.C. Kwon, S.Y. Jeong, O.F. Silvestre, X. Chen, Y. Hwang, E. Kim, S.C. Lee, M.I.N.E.T. Al, pH-controlled gas-generating mineralized nanoparticles: a theranostic agent for ultrasound imaging and therapy of cancers, ACS Nano 9 (2015) 134–145.
[36] M. Horie, K. Nishio, H. Kato, S. Endoh, K. Fujita, A. Nakamura, S. Kinugasa, Y. Hagihara, Y. Yoshida, H. Iwahashi, Evaluation of cellular influences caused by calcium carbonate nanoparticles, Chem. Biol. Interact. 210 (2014) 64–76.
[37] A. Som, R. Raliya, L. Tian, W. Akers, J. Ippolito, S. Singamaneni, P. Biswas, S. Achilefu, Monodispersed calcium carbonate nanoparticles modulate local pH and inhibit tumor growth in vivo, Nano 8 (2016) 12639–12647.
[38] A. Shafiu Kamba, M. Ismail, T.A. Tengku Ibrahim, Z.A.B. Zakaria, A pH-sensitive, biobased calcium carbonate aragonite nanocrystal as a novel anticancer delivery system, Biomed. Res. Int. 2013 (2013) 1–10.
[39] J.A. Lee, M.K. Kim, H.M. Kim, J.K. Lee, J. Jeong, Y.R. Kim, J.M. Oh, S.J. Choi, The fate of calcium carbonate nanoparticles administered by oral route: absorption and their interaction with biological matrices, Int. J. Nanomedicine 10 (2015) 2273–2293.
[40] M.S. Jeong, H.S. Cho, S.J. Park, K.S. Song, K.S. Ahn, M.H. Cho, J.S. Kim, Physico-chemical characterization-based safety evaluation of nanocalcium, Food Chem. Toxicol. 62 (2013) 308–317.
[41] F. Tewes, O.L. Gobbo, C. Ehrhardt, A.M. Healy, Amorphous calcium carbonate based-microparticles for peptide pulmonary delivery, ACS Appl. Mater. Interfaces 8 (2016) 1164–1175.
[42] J. Li, H. Jiang, X. Ouyang, S. Han, J. Wang, R. Xie, W. Zhu, N. Ma, H. Wei, Z. Jiang, $CaCO_3$/tetraethylenepentamine–graphene hollow microspheres as biocompatible bone drug carriers for controlled release, ACS Appl. Mater. Interfaces 8 (2016) 30027–30036.
[43] Y.I. Svenskaya, A.M. Pavlov, D.A. Gorin, D.J. Gould, B.V. Parakhonskiy, G.B. Sukhorukov, Photodynamic therapy platform based on localized delivery of photosensitizer by Vaterite submicron particles, Colloids Surf. B Biointerfaces 146 (2016) 171–179.
[44] T. Cheang, S. Wang, Z. Hu, Z. Xing, G. Chang, C. Yao, Y. Liu, H. Zhang, A.-W. Xu, Calcium carbonate/CaIP6 nanocomposite particles as gene delivery vehicles for human vascular smooth muscle cells, J. Mater. Chem. 20 (2010) 8050–8055.
[45] J. Wei, T. Cheang, B. Tang, H. Xia, Z. Xing, Z. Chen, Y. Fang, W. Chen, A. Xu, S. Wang, J. Luo, The inhibition of human bladder cancer growth by calcium carbonate/CaIP6 nanocomposite particles delivering AIB1 siRNA, Biomaterials 34 (2013) 1246–1254.
[46] C. Qi, Y.J. Zhu, F. Chen, Microwave hydrothermal transformation of amorphous calcium carbonate nanospheres and application in protein adsorption, ACS Appl. Mater. Interfaces 6 (2014) 4310–4320.
[47] Y. Zhao, Z. Luo, M. Li, Q. Qu, X. Ma, S. Yu, Y. Zhao, A preloaded amorphous calcium carbonate/doxorubicin@silica nanoreactor for pH-responsive delivery of an anticancer drug, Angew. Chem. Int. Ed. 54 (2015) 919–922.
[48] Y. Zhao, L.N. Lin, Y. Lu, S.F. Chen, L. Dong, S.H. Yu, Templating synthesis of preloaded doxorubicin in hollow mesoporous silica nanospheres for biomedical applications, Adv. Mater. 22 (2010) 5255–5259, http://dx.doi.org/10.1002/adma.201002395.
[49] Z. Dong, L. Feng, W. Zhu, X. Sun, M. Gao, H. Zhao, Y. Chao, Z. Liu, $CaCO_3$ nanoparticles as an ultra-sensitive tumor-pH-responsive nanoplatform enabling real-time drug release monitoring and cancer combination therapy, Biomaterials 110 (2016) 60–70.
[50] X. Ying, C. Shan, K. Jiang, Z. Chen, Y. Du, Intracellular pH-sensitive delivery $CaCO_3$ nanoparticles templated by hydrophobic modified starch micelles, RSC Adv. 4 (2014) 10841–10844.
[51] J.D. Snook, C.B. Chesson, A.G. Peniche, S.M. Dann, A. Paulucci, I.V. Pinchuk, J.S. Rudra, Peptide nanofiber–$CaCO_3$ composite microparticles as adjuvant-free oral vaccine delivery vehicles, J. Mater. Chem. B 4 (2016) 1640–1649.
[52] D. Liu, G. Jiang, W. Yu, L. Li, Z. Tong, X. Kong, J. Yao, Oral delivery of insulin using $CaCO_3$-based composite nanocarriers with hyaluronic acid coatings, Mater. Lett. 188 (2017) 263–266.
[53] J. Lee, H.-S. Min, D.G. You, K. Kim, I.C. Kwon, T. Rhim, K.Y. Lee, Theranostic gas-generating nanoparticles for targeted ultrasound imaging and treatment of neuroblastoma, J. Control. Release 223 (2016) 197–206.
[54] X. He, T. Liu, Y. Chen, D. Cheng, X. Li, Y. Xiao, Y. Feng, Calcium carbonate nanoparticle delivering vascular endothelial growth factor-C siRNA effectively inhibits lymphangiogenesis and growth of gastric cancer in vivo, Cancer Gene Ther. 15 (2008) 193–202.
[55] S. Chen, D. Zhao, F. Li, R.-X. Zhuo, S.-X. Cheng, Co-delivery of genes and drugs with nanostructured calcium carbonate for cancer therapy, RSC Adv. 2 (2012) 1820–1826.
[56] S.K. Kim, M.B. Foote, L. Huang, Targeted delivery of EV peptide to tumor cell cytoplasm using lipid coated calcium carbonate nanoparticles, Cancer Lett. 334 (2013) 311–318.
[57] S. Chen, F. Li, R.-X. Zhuo, S.-X. Cheng, Efficient non-viral gene delivery mediated by nanostructured calcium carbonate in solution-based transfection and solid-phase transfection, Mol. BioSyst. 7 (2011) 2841–2847.
[58] D. Zhao, R.-X. Zhuo, S.-X. Cheng, Modification of calcium carbonate based gene and drug delivery systems by a cell-penetrating peptide, Mol. BioSyst. 8 (2012) 3288–3294.
[59] C.-Q. Wang, J.-L. Wu, R.-X. Zhuo, S.-X. Cheng, Protamine sulfate-calcium carbonate-plasmid DNA ternary nanoparticles for efficient gene delivery, Mol. BioSyst. 10 (2014) 672–678.
[60] J.-L. Wu, C.-Q. Wang, R.-X. Zhuo, S.-X. Cheng, Multi-drug delivery system based on alginate/calcium carbonate hybrid nanoparticles for combination chemotherapy, Colloids Surf. B Biointerfaces 123 (2014) 498–505.
[61] J.-L. Wu, X.-Y. He, P.-Y. Jiang, M.-Q. Gong, R.-X. Zhuo, S.-X. Cheng, Biotinylated carboxymethyl chitosan/$CaCO_3$ hybrid nanoparticles for targeted drug delivery to overcome tumor drug resistance, RSC Adv. 6 (2016) 69083–69093.
[62] F. Kong, H. Zhang, X. Zhang, D. Liu, D. Chen, W. Zhang, L. Zhang, H.A. Santos, M. Hai, Biodegradable Photothermal and pH responsive calcium carbonate@phospholipid@acetalated dextran hybrid platform for advancing biomedical applications, Adv. Funct. Mater. 26 (2016) 6158–6169.
[63] B.V. Parakhonsky, M. Zyuzin, A.M. Yashchenok, S. Carregal-romero, J. Rejman, H. Möhwald, W.J. Parak, A. Skirtach, The influence of the size and aspect ratio of anisotropic, porous $CaCO_3$ particles on their uptake by cells, J Nanobiotechnol. 13 (2015) 13–53.
[64] S. Huang, J.C. Chen, C.W. Hsu, W.H. Chang, Effects of nano calcium carbonate and nano calcium citrate on toxicity in ICR mice and on bone mineral density in an ovariectomized mice model, Nanotechnology 20 (2009) 375102.
[65] M.-K. Kim, J.-A. Lee, M.-R. Jo, M.-K. Kim, H.-M. Kim, J.-M. Oh, N. Song, S.-J. Choi, Cytotoxicity, uptake behaviors, and oral absorption of food grade calcium carbonate nanomaterials, Nano 5 (2015) 1938–1954.
[66] M. Björnmalm, M. Faria, F. Caruso, Increasing the impact of materials in and beyond bio-nano science, J. Am. Chem. Soc. 138 (2016) 13449–13456.
[67] V. Lauth, M. Maas, K. Rezwan, Coacervate-directed synthesis of $CaCO_3$ microcarriers for pH-responsive delivery of biomolecules, J. Mater. Chem. B 2 (2014) 7725–7731.
[68] B.V. Parakhonskiy, A. Haase, R. Antolini, Sub-micrometer vaterite containers: synthesis, substance loading, and release, Angew. Chem. Int. Ed. 51 (2012) 1195–1197.
[69] D.B. Trushina, T.V. Bukreeva, M.N. Antipina, Size-controlled synthesis of vaterite calcium carbonate by the mixing method: aiming for nanosized particles, Cryst. Growth Des. 16 (2016) 1311–1319.
[70] M. Cocquyt, B. Pinchasik, D. Khalenkow, H. Mo, M. Konrad, A. Skirtach, Loading capacity versus enzyme activity in anisotropic and spherical vaterite microparticles, ACS Appl. Mater. Interfaces 8 (2016) 14284–14292.
[71] S. Shahabi, S. Döscher, T. Bollhorst, L. Treccani, M. Maas, R. Dringen, K. Rezwan, Enhancing cellular uptake and doxorubicin delivery of mesoporous silica nanoparticles via surface functionalization: effects of serum, ACS Appl. Mater. Interfaces 7 (2015) 26880–26891.

[72] K. Apte, R. Stick, M. Radmacher, Mechanics in human fibroblasts and progeria: lamin A mutation E145K results in stiffening of nuclei, J. Mol. Recognit. 30 (2017) 1–11.
[73] P. Kaempfe, V.R. Lauth, T. Halfer, L. Treccani, M. Maas, K. Rezwan, Micromolding of calcium carbonate using a bio-inspired, coacervation-mediated process, J. Am. Ceram. Soc. 96 (2013) 736–742.
[74] V. Vergaro, P. Papadia, S. Leporatti, S.A. De Pascali, F.P. Fanizzi, G. Ciccarella, Synthesis of biocompatible polymeric nano-capsules based on calcium carbonate: a potential cisplatin delivery system, J. Inorg. Biochem. 153 (2015) 284–292.
[75] C. Graf, Q. Gao, I. Schütz, C.N. Noufele, W. Ruan, U. Posselt, E. Korotianskiy, D. Nordmeyer, F. Rancan, S. Hadam, A. Vogt, J. Lademann, V. Haucke, E. Rühl, Surface functionalization of silica nanoparticles supports colloidal stability in physiological media and facilitates internalization in cells, Langmuir 28 (2012) 7598–7613.
[76] L.B. Gower, D.J. Odom, Deposition of calcium carbonate films by a polymer-induced liquid-precursor (PILP) process, J. Cryst. Growth 210 (2000) 719–734.
[77] J.S. Evans, "Liquid-like" biomineralization protein assemblies: a key to the regulation of non-classical nucleation, CrystEngComm 15 (2013) 8388–8394.
[78] H.-B. Yao, J. Ge, L.-B. Mao, Y.-X. Yan, S.-H. Yu, 25th anniversary article: artificial carbonate nanocrystals and layered structural nanocomposites inspired by nacre: synthesis, fabrication and applications, Adv. Mater. 26 (2014) 163–188.
[79] A.I. Petrov, D.V. Volodkin, G.B. Sukhorukov, Protein-calcium carbonate coprecipitation: a tool for protein encapsulation, Biotechnol. Prog. 21 (2005) 918–925.
[80] T.L. Moore, L. Rodriguez-Lorenzo, V. Hirsch, S. Balog, D. Urban, C. Jud, B. Rothen-Rutishauser, M. Lattuada, A. Petri-Fink, Nanoparticle colloidal stability in cell culture media and impact on cellular interactions, Chem. Soc. Rev. 44 (2015) 6287–6305.
[81] N. Nafee, M. Schneider, U.F. Schaefer, C.-M. Lehr, Relevance of the colloidal stability of chitosan/PLGA nanoparticles on their cytotoxicity profile, Int. J. Pharm. 381 (2009) 130–139.
[82] M. Horie, K. Nishio, K. Fujita, H. Kato, S. Endoh, M. Suzuki, A. Nakamura, A. Miyauchi, S. Kinugasa, K. Yamamoto, H. Iwahashi, H. Murayama, E. Niki, Y. Yoshida, Cellular responses by stable and uniform ultrafine titanium dioxide particles in culture-medium dispersions when secondary particle size was 100nm or less, Toxicol. in Vitro 24 (2010) 1629–1638.
[83] S. Maeno, Y. Niki, H. Matsumoto, H. Morioka, T. Yatabe, A. Funayama, Y. Toyama, T. Taguchi, J. Tanaka, The effect of calcium ion concentration on osteoblast viability, proliferation and differentiation in monolayer and 3D culture, Biomaterials 26 (2005) 4847–4855.
[84] C. Kusonwiriyawong, P. Van De Wetering, J.A. Hubbell, H.P. Merkle, E. Walter, Evaluation of pH-dependent membrane-disruptive properties of poly(acrylic acid) derived polymers, Eur. J. Pharm. Biopharm. 56 (2003) 237–246.